Connecting chaos in the Coupled Brusselator System

F. Drubi[a], A. Mayora-Cebollero[b], C. Mayora-Cebollero[b], S. Ibáñez[a], J.A. Jover-Galtier[b], Á. Lozano[c], L. Pérez[a], R. Barrio[b]

[a] *Dpto. Matemáticas. University of Oviedo, E-33007 Oviedo, Spain*
[b] *IUMA, CoDy and Dpto. Matemática Aplicada. Universidad de Zaragoza, E-50009 Zaragoza, Spain*
[c] *IUMA, CoDy and Dpto. Matemáticas. Universidad de Zaragoza, E-50009 Zaragoza, Spain*

Abstract

A family of vector fields describing two Brusselators linearly coupled by diffusion is considered. This model is a well-known example of how identical oscillatory systems can be coupled with a simple mechanism to create chaotic behavior. In this paper we discuss the relevance and possible relation of two chaotic regions. One of them is located using numerical techniques. The another one was first predicted by theoretical results and later studied via numerical and continuation techniques. As a conclusion, under the constrains of our exploration, both regions are not connected and, moreover, the former one has a big size, whereas the later one is quite small and hence, it might not be detected without the support of theoretical results. Our analysis includes a detailed analysis of singularities and local bifurcations that permits to provide a global parametric study of the system.

Keywords: Coupled systems, Brusselator model, chaos, bifurcations

Email addresses: drubifatima@uniovi.es (F. Drubi), amayora@unizar.es (A. Mayora-Cebollero), cmayora@unizar.es (C. Mayora-Cebollero), mesa@uniovi.es (S. Ibáñez), jorgejover@unizar.es (J.A. Jover-Galtier), alozano@unizar.es (Á. Lozano), perezplucia@uniovi.es (L. Pérez), rbarrio@unizar.es (R. Barrio)

2000 MSC: 34C15, 37D45, 37G10, 37G15

1. Introduction

Many phenomena in nature can be modeled in terms of the interaction among elementary dynamical units. A neural network, either biological or artificial, is a paradigmatic example. Each neuron communicates with its neighbors in the network through electrochemical signals giving rise to dynamical systems exhibiting an extraordinary complexity. Another classical context, which is the one that we consider in this paper, is that provided by chemical reactors where substances can move from one reactor to another according to simple rules (see, for instance, [1, 2]).

Among the many questions that can be asked when studying coupled systems, here we are mainly focused on how simple couplings of simple dynamics can generate complex behaviors. In particular, we consider homogeneous networks of differential equations linearly coupled by diffusion

$$\mathbf{u}_i' = F(\mathbf{u}_i) + \sum_{j=1}^{r} a_{ij}\Lambda(\mathbf{u}_j - \mathbf{u}_i), \tag{1}$$

where $\mathbf{u}_i \in \mathbb{R}^k$ for each $i = 1, \ldots, r$; $a_{ij} = a_{ji} \in \{0, 1\}$; Λ is a $k \times k$ diagonal matrix; and F is a C^∞ family of vector fields.

The seminal work of Turing [1], where he studied the arising of oscillatory behavior in a ring of diffusively coupled linear systems, led Smale [2] to wonder whether globally attracting periodic orbits could be generated in a model of identical differential equations linearly coupled by diffusion when the internal dynamics of each uncoupled system reduces to a globally attracting equilibrium point. Indeed, Smale provided an example of such dynamical behavior with two identical 4-dimensional systems linearly coupled by diffusion. Later, other examples were given but coupling identical systems of dimension 2 or 3 [3, 4]. With the stimuli provided by all these results, it is worth asking what other dynamics can be generated through diffusion processes and, in particular, the possibility of chaotic behaviors emerging. A positive answer to this question was given in [5], where authors proved the existence of strange attractors in a model consisting of two Brusselators linearly coupled by diffusion.

The Brusselator is a theoretical model of a chemical reaction introduced by Prigogine et al. [6]:

$$\begin{cases} x' &= A - (B+1)x + x^2 y, \\ y' &= Bx - x^2 y, \end{cases} \tag{2}$$

with A, B positive constants. This system exhibits quite simple dynamics: first quadrant is invariant, and there is a supercritical Hopf bifurcation when $B = A^2 + 1$. When $B < A^2 + 1$ there is a unique globally attracting equilibrium point at $(A, B/A)$, and if $B > A^2 + 1$ there is a unique globally attracting periodic orbit.

Based on this model, in [5] a system composed of two coupled Brusselators, with coupling parameters λ_1 and λ_2, is proposed:

$$\begin{cases} x_1' &= A - (B+1)x_1 + x_1^2 y_1 + \lambda_1(x_2 - x_1), \\ y_1' &= Bx_1 - x_1^2 y_1 + \lambda_2(y_2 - y_1), \\ x_2' &= A - (B+1)x_2 + x_2^2 y_2 + \lambda_1(x_1 - x_2), \\ y_2' &= Bx_2 - x_2^2 y_2 + \lambda_2(y_1 - y_2). \end{cases} \tag{3}$$

Notice that (3) is a simple example of the general formulation given in (1). We refer to (3) as the Coupled Brusselator System, `CBS` in the sequel. All parameters in (3) are positive, and in the absence of interaction, i.e., when $\lambda_1 = \lambda_2 = 0$, we have two isolated identical Brusselators.

Numerical evidences of the existence of chaotic behavior in model (3) had been previously found in [7]. However, arguments used in [5] to show the existence of strange attractors in (3) are analytic. Namely, it was argued the existence of a local bifurcation (a 3-dimensional nilpotent singularity of codimension 3) that unfolds Shilnikov homoclinic bifurcations. It is well-known that these global bifurcations imply the appearance of strange attractors. We explain all these technical details in Section 2.

One of the goals of this paper is to elucidate whether there is a relation between the chaotic region found by Schreiber and Marek [7], `SM` in what follows, and the one detected by Drubi, Ibáñez and Rodríguez [5], hereinafter denoted as `DIR`. In Figure 1, the chaotic attractors of both regions are illustrated. Since `SM` and `DIR` are contained in two different parametric planes with A and λ_2 fixed, we consider a one-parameter family of (B, λ_1)-planes that links both. Within this framework, we show that there is no connection between them, namely, `SM` can be continued up to a region in the plane containing `DIR`, but not meeting `DIR`. Most importantly, we observe a notable difference in the size of these two zones in the parameter space; `SM` is large while `DIR` is very small. Then, the chaotic region `SM` is globally more relevant than the chaotic region `DIR`. However, we have located another small chaotic region in the biparametric plane of `DIR`, and the presence of several small chaotic regions may be of special relevance. We especially highlight the fact that only analytical tools allow us to detect numerically the small-sized chaotic dynamics, which would otherwise go unnoticed with numerical ex-

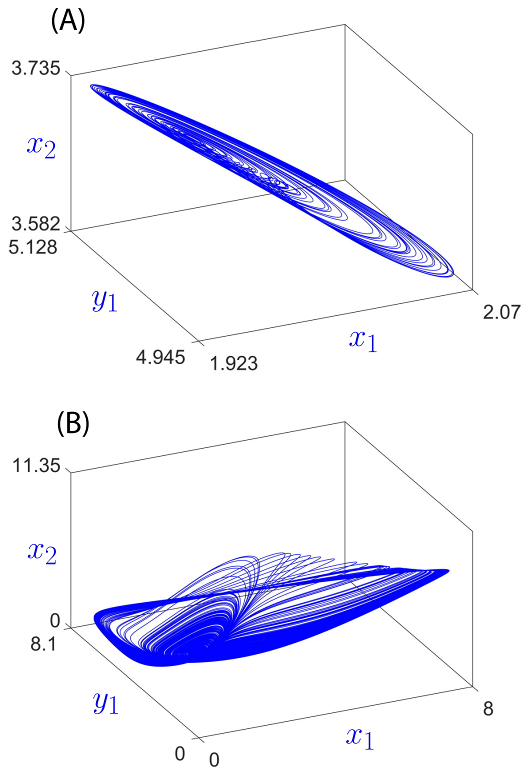

Figure 1: 3-D representation of chaotic attractors. (A) Chaotic attractor of `DIR` region with $A = 2.828812321130726$, $B = 11.479799259891854$, $\lambda_1 = 1.2055$, $\lambda_2 = 1.679725368058570$, and $(x_1, y_1, x_2, y_2) = (2.057176, 4.956813, 3.600131, 3.390639)$. (B) Chaotic attractor of `SM` region with $A = 2.0$, $B = 6.375300171526684$, $\lambda_1 = 1.2$, $\lambda_2 = 80.0$, and $(x_1, y_1, x_2, y_2) = (1.9, 3.0, 2.1, 2.9)$.

plorations alone. Therefore, the location of `DIR` has a remarkable theoretical interest.

Structure of the paper is as follows. In Section 2 we describe the analytical tools that allow us to prove the existence of chaotic behaviors in a given family of vector fields. Singularities arising in the `CBS` are discussed in Section 3. We include both, a global analysis of singularities and partial bifurcation diagrams that extend the theoretical results. These diagrams are obtained with MatCont [8]. The map of local bifurcations includes nilpotent cases [5, 9] and also Hopf-Pitchfork singularities [10]. Numerical results are provided in Section 4. They include 2-parameter studies of the chaotic regions `SM` and `DIR` that show, among other details, the different size of the regions. A three-parameter continuation analysis performed using AUTO [11] shows that both regions are not connected.

2. Theoretical results: Singularities and chaos

Literature is plenty of examples where numerical analysis permits arguing the existence of chaotic dynamics in given families of dynamical systems [12, 13, 14]. Conversely, proofs based on the use of analytical tools are uncommon. However, nowadays there exist methods that can be of general use when proving the existence of chaos in the case of families of vector fields. We refer to the study of singularities, those ones that unfold global configurations that explain the genesis of strange attractors. An extensive discussion about the relationship between singularities and chaos can be found in [15]. Recall that an attractor is said chaotic if it contains a dense orbit with a positive Lyapunov exponent. This last condition explains why orbits diverge within the attractor or, in other words, the high sensitivity of the system to initial conditions. Before understanding the aforementioned tools, we have to comment some results about the existence of strange attractors in maps.

In [16], Benedicks and Carleson proved the existence of strange attractors in the Hénon family for a positive measure set of parameter values. Later on, using techniques introduced in [16], Mora and Viana [17] proved that in any generic 1-parameter family of 2-dimensional diffeomorphisms unfolding a point of homoclinic tangency, there exists a positive measure set of parameters for which the diffeomorphism exhibits (Hénon-like) strange attractors. By point of homoclinic tangency we mean any quadratic tangency between the invariant manifolds of a saddle type fixed point.

Now, assume that X is a 3-dimensional vector field with a saddle-focus equilibrium point p whose eigenvalues λ and $-\rho \pm i\omega$ satisfy $\lambda > \rho > 0$. Under these conditions, a homoclinic orbit $\gamma(t)$ such that $\lim_{t\to\pm\infty} \gamma(t) = p$ is said of Shilnikov type. In [18], Shilnikov proved the existence of infinitely many periodic orbits of saddle type in each neighborhood of the homoclinic orbit. Later, in [19, 20], it was proved that the first return map around the homoclinic orbit exhibits an infinity of Smale horseshoes. Each horseshoe map contains an infinite number of transverse homoclinic points, that is, points where the invariant manifolds of a saddle type fixed point meet transversely. When the vector field is unfolded to create a homoclinic bifurcation, horseshoes are destroyed in processes where transverse intersections are created/destroyed in pairs through homoclinic tangencies. Therefore, the existence of strange attractors follows from [17] (see also [21, 22, 23]).

On the other hand, in [24] (see also [25, 26], and [27] for additional related technical details), it was proved that Shilnikov homoclinic bifurcations, and hence Hénon-like strange attractors, arise in any generic unfolding of a 3-dimensional nilpotent singularity of codimension 3, that is, a singularity where the 1-jet is linearly conjugated to

$$x' = y, \qquad y' = z, \qquad z' = 0.$$

The essential argument is the fact that any generic unfolding can be written as a perturbation of a vector field exhibiting a Bykov cycle, that is, a heteroclinic cycle formed by two saddle-focus equilibria with different stability indexes, two branches of the 1-dimensional invariant manifolds are coincident and the two-dimensional invariant manifolds intersect transversely. A Bykov cycle is a codimension-two configuration which generically unfolds Shilnikov homoclinic orbits and hence, the existence of nilpotent singularities implies the emergence of chaotic behavior in a given family.

There exist other singularities that unfold chaotic dynamics. In fact, three is not the lowest codimension that it is required to achieve this. Indeed, as it has been argued in [28, 29] (see also references therein), there exist Hopf-Zero singularities of codimension 2 which generically unfold Shilnikov homoclinic orbits. However, from the point of view of applications, one should notice that part of the required generic conditions depends on the full jet of the singularity and they must be checked with numerical techniques.

Remark 1. Although the detection of the appropriate singularities is an user-friendly tool to prove the existence of chaotic behavior in a given family, the method does not provide a precise location of chaotic dynamics neither in the phase-space nor in the parameter space. In order to illustrate the chaotic behavior numerically, an alternative method must be used.

3. Study of singularities and bifurcations

The `CBS` (3) has an equilibrium point at $(A, B/A, A, B/A)$ for all parameter values (the trivial equilibrium point). It belongs to the invariant plane $\Pi = \{x_1 = x_2, y_1 = y_2\}$. The dynamics on this invariant plane corresponds to that of two isolated Brusselators. Moreover, it easily follows that the `CBS` is invariant under the symmetry

$$(x_1, y_1, x_2, y_2) \to (x_2, y_2, x_1, y_1). \tag{4}$$

For simplicity, we consider a change of variables given by $\xi_1 = (x_2 - x_1)/2$, $\xi_2 = (y_2 - y_1)/2$, $\eta_1 = (x_2 + x_1)/2$, and $\eta_2 = (y_2 + y_1)/2$. In the new coordinates, the `CBS` takes the form

$$\begin{cases} \xi_1' = -(B+1)\xi_1 + (\eta_1^2 + \xi_1^2)\xi_2 + 2\eta_1\eta_2\xi_1 - 2\lambda_1\xi_1, \\ \xi_2' = B\xi_1 - (\eta_1^2 + \xi_1^2)\xi_2 - 2\eta_1\eta_2\xi_1 - 2\lambda_2\xi_2, \\ \eta_1' = A - (B+1)\eta_1 + (\eta_1^2 + \xi_1^2)\eta_2 + 2\xi_1\xi_2\eta_1, \\ \eta_2' = B\eta_1 - (\eta_1^2 + \xi_1^2)\eta_2 - 2\xi_1\xi_2\eta_1. \end{cases} \tag{5}$$

Notice that, with respect to these new variables, the trivial equilibrium point is $(0, 0, A, B/A)$ and the invariant plane is rewritten as $\Pi = \{\xi_1 = 0,\ \xi_2 = 0\}$.

In [5], it is proved that all equilibrium points of (5) satisfy the relations below

$$\xi_2 = -\frac{(1+2\lambda_1)\xi_1}{2\lambda_2}, \quad \eta_1 = A, \quad \eta_2 = \frac{AB\lambda_2 + A(1+2\lambda_1)\xi_1^2}{(A^2+\xi_1^2)\lambda_2}, \tag{6}$$

where $A^2 + \xi_1^2 \neq 0$ since $A > 0$, and ξ_1 is a solution of the fifth-degree polynomial equation

$$\xi_1\,(\xi_1^4 + (2A^2 + p)\xi_1^2 + A^4 + A^2 p + q) = 0, \tag{7}$$

with

$$p = \frac{2\lambda_2(B + 2\lambda_1 + 1) - 4A^2(1+2\lambda_1)}{1+2\lambda_1} \quad \text{and} \quad q = \frac{4A^2(A^2(1+2\lambda_1) - B\lambda_2)}{1+2\lambda_1}.$$

Lemma 1. *Let*

$$\begin{aligned}
\mathcal{V}_1 &= \{(A,B,\lambda_1,\lambda_2) \in V : A^4 + A^2p + q > 0,\ 2A^2 + p > -2\sqrt{A^4 + A^2p + q}\},\\
\mathcal{V}_2 &= \{(A,B,\lambda_1,\lambda_2) \in V : A^4 + A^2p + q < 0\},\\
\mathcal{V}_3 &= \{(A,B,\lambda_1,\lambda_2) \in V : A^4 + A^2p + q > 0,\ 2A^2 + p < -2\sqrt{A^4 + A^2p + q}\},
\end{aligned}$$

where $V = \{(A,B,\lambda_1,\lambda_2) \in \mathbb{R}^4 :\ A > 0,\ B > 0,\ \lambda_1 > 0,\ \lambda_2 > 0\}$.

1. *If* $(A,B,\lambda_1,\lambda_2) \in \mathcal{V}_1$, *the* **CBS** *in (5) has only one equilibrium point: the trivial singularity* $(0,0,A,B/A)$, *which undergoes a supercritical Hopf bifurcation when* $B = A^2 + 1$.
2. *If* $(A,B,\lambda_1,\lambda_2) \in \mathcal{V}_2$, *the* **CBS** *in (5) has three equilibrium points: the trivial singularity and* $Q_\pm = (\xi^\pm_{1,q}, \xi^\pm_{2,q}, \eta^\pm_{1,q}, \eta^\pm_{2,q})$ *with*

$$\xi^\pm_{1,q} \quad = \quad \pm\sqrt{\frac{A^2(1+2\lambda_1) - \lambda_2 - B\lambda_2 - 2\lambda_1\lambda_2 + \sqrt{\lambda_2\left(-4\left(A + 2A\lambda_1\right)^2 + \left(1 + B + 2\lambda_1\right)^2\lambda_2\right)}}{1 + 2\lambda_1}}$$

   and $\xi^\pm_{2,q}$, $\eta^\pm_{1,q}$, *and* $\eta^\pm_{2,q}$ *provided by formulas in (6).*
3. *If* $(A,B,\lambda_1,\lambda_2) \in \mathcal{V}_3$, *the* **CBS** *has five equilibrium points: the trivial singularity, the points* $Q_\pm$ *defined above and* $P_\pm = (\xi^\pm_{1,p}, \xi^\pm_{2,p}, \eta^\pm_{1,p}, \eta^\pm_{2,p})$ *with*

$$\xi^\pm_{1,p} \quad = \quad \pm\sqrt{\frac{A^2(1+2\lambda_1) - \lambda_2 - B\lambda_2 - 2\lambda_1\lambda_2 - \sqrt{\lambda_2\left(-4\left(A + 2A\lambda_1\right)^2 + \left(1 + B + 2\lambda_1\right)^2\lambda_2\right)}}{1 + 2\lambda_1}}$$

   and $\xi^\pm_{2,p}$, $\eta^\pm_{1,p}$, *and* $\eta^\pm_{2,p}$ *provided by formulas in (6).*

Proof. Write the second factor on the left hand side of (7) as $\xi_1^4 + \beta\xi_1^2 + \gamma$ with $\beta = 2A^2 + p$ and $\gamma = A^4 + A^2p + q$. The result follows immediately taking into account that any $z^2 + \beta z + \gamma = 0$ has no positive real root for $\gamma > 0$ and $\beta > -\sqrt{4\gamma}$; one positive real root for $\gamma < 0$; and two positive real roots for $\gamma > 0$ and $\beta < -\sqrt{4\gamma}$. $\square$

Furthermore, we note that the singularities $P_\pm$ and $Q_\pm$ also undergo Hopf bifurcations but their hypersurface expressions are too long to be included here.

In summary, there always exists the trivial singularity in the `CBS` (5), which stays on the invariant plane $\Pi = \{\xi_1 = 0, \xi_2 = 0\}$, but two or four nontrivial singularities, which are symmetric with respect to Π, can appear when parameters A, B, λ_1 and λ_2 satisfy the conditions stated in Lemma 1.

3.1. Local bifurcations at the trivial singularity

The characteristic polynomial of the Jacobian matrix at $(0, 0, A, B/A)$ associated to (5) can be written as $P(\mu) = (\mu^2 + c_1\mu + c_0)(\mu^2 + d_1\mu + d_0)$, where $c_1 = 1 + A^2 - B + 2\lambda_1 + 2\lambda_2$, $c_0 = A^2(1 + 2\lambda_1) + 2\lambda_2(1 + 2\lambda_1 - B)$, $d_1 = 1 + A^2 - B$, and $d_0 = A^2$.

Remark 2. We are only interested in all possible bifurcations for an equilibrium point under conditions of $\mathbb{Z}_2$-symmetry.

The Jacobian matrix has at least one zero eigenvalue for all parameter values in

$$\mathcal{P} = \left\{(A, B, \lambda_1, \lambda_2) \in V : B = (A^2 + 2\lambda_2)(1 + 2\lambda_1)/(2\lambda_2)\right\}.$$

Therefore, under some additional open conditions, the `CBS` (5) undergoes a Pitchfork bifurcation at the trivial singularity $(0, 0, A, B/A)$ on the bifurcation hypersurface $\mathcal{P}$, which is the transition from $\mathcal{V}_1$ to $\mathcal{V}_2$ or from $\mathcal{V}_2$ to $\mathcal{V}_3$. On the other hand, there exists a bifurcation surface on $\mathcal{P}$,

$$\mathcal{DZ}_0 = \left\{(A, B, \lambda_1, \lambda_2) \in \mathcal{P} : B = 1 + A^2 + 2\lambda_1 + 2\lambda_2\right\},$$

such that the Jacobian matrix of (5) at the trivial singularity has a double zero eigenvalue with geometric multiplicity one and a pair of eigenvalues with nonzero real part. Up to degenerations at the higher order terms, $\mathcal{DZ}_0$ is a bifurcation surface of codimension 2. There is no parameter value for which the trivial singularity has a 2-dimensional center manifold with a restricted linear part identically zero.

The Jacobian matrix has at least a pair of pure imaginary eigenvalues on the bifurcation hypersurfaces of codimension 1,

$$\mathcal{H}_1 = \left\{(A, B, \lambda_1, \lambda_2) \in V : \quad B = 1 + A^2 + 2(\lambda_1 + \lambda_2),\ \lambda_1 > \tfrac{4\lambda_2^2 + 2\lambda_2 A^2 - A^2}{2A^2}\right\},$$

which corresponds to the Hopf bifurcations occurring transversally to Π, and

$$\mathcal{H}_2 = \left\{(A, B, \lambda_1, \lambda_2) \in V : B = 1 + A^2,\ A^2(1 + 2\lambda_1 - 2\lambda_2) + 4\lambda_1\lambda_2 \neq 0\right\},$$

which corresponds to Hopf bifurcation for the isolated Brusselator system on the invariant plane Π.

The hypersurfaces $\mathcal{P}$ and $\mathcal{H}_2$ have a common border along the bifurcation surface

$$\mathcal{HP} = \left\{(A, B, \lambda_1, \lambda_2) \in V : B = 1 + A^2,\ \lambda_1 = \frac{(-1 + 2\lambda_2)A^2}{2(A^2 + 2\lambda_2)},\ \lambda_2 > \frac{1}{2}\right\}$$

on which the Jacobian matrix at $(0, 0, A, B/A)$ has a pair of pure imaginary eigenvalues and a zero eigenvalue. Therefore, $\mathcal{HP}$ is a bifurcation surface of Hopf-Pitchfork singularities of codimension at least 2. In [10], it is proved that several cases of codimension 2, 3 and 4 are generically unfolded by the `CBS`.

Finally, the Jacobian matrix has two pairs of pure imaginary eigenvalues when the `CBS` is uncoupled ($\lambda_1 = \lambda_2 = 0$) and $B = A^2 + 1$. Although it is an

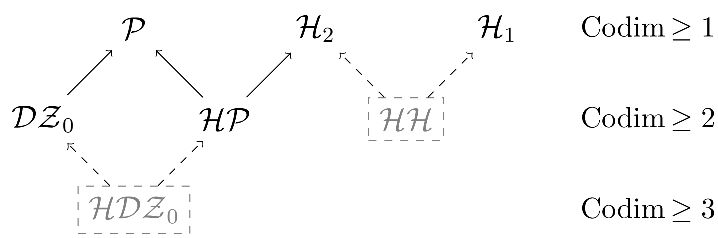

Figure 2: Local bifurcations scheme (arrows indicate that a local bifurcation is unfolded by other of higher codimension): Pitchfork ($\mathcal{P}$), Hopf ($\mathcal{H}_i$, $i = 1, 2$), Double-Zero ($\mathcal{DZ}_0$), Hopf-Pitchfork ($\mathcal{HP}$), Hopf-Hopf ($\mathcal{HH}$), and Hopf-Double-Zero ($\mathcal{HDZ}_0$) bifurcations for the trivial singularity. Bifurcations framed in a dashed box correspond to parameter values on the boundary of V.

interesting configuration, it appears for parameter values on the boundary of V. In [30], this problem was studied in the context of linear diffusion couplings of two Hopf bifurcations. Other degenerate cases for the eigenvalues of the Jacobian matrix at the trivial singularity of (5) occur when $A = 0$. Although these degenerate configurations (Hopf-Hopf and Hopf-Double-Zero bifurcations, denoted by $\mathcal{HH}$ and $\mathcal{HDZ}_0$, respectively) may be important, the techniques that are used exceed the classical ones of the local bifurcation theory and belong to the context of singular perturbation problems.

In Figure 2, we sketch the set of bifurcations described above.

3.2. Local bifurcations at the nontrivial singularities

The `CBS` in (5) has exactly three singularities for parameter values on the hypersurface of codimension 1,

$$\mathcal{SN} = \left\{ (A, B, \lambda_1, \lambda_2) \in V : \lambda_2 = \frac{4A^2(1 + 2\lambda_1)^2}{(1 + B + 2\lambda_1)^2},\ B > 3 + 6\lambda_1 \right\}, \tag{8}$$

the trivial singularity and two nonhyperbolic equilibria $S^{\pm} = (\xi_1^{\pm}, \xi_2^{\pm}, \eta_1^{\pm}, \eta_2^{\pm})$

with $\xi_2^{\pm}$, $\eta_1^{\pm}$ and $\eta_2^{\pm}$ provided in (6) and

$$\xi_1^{\pm} = \pm\sqrt{\frac{A^2(-3+B-6\lambda_1)}{1+B+2\lambda_1}}.$$

The equilibrium points $S^{\pm}$ undergo a saddle-node bifurcation for parameter values on $\mathcal{SN}$, if the appropriate open conditions are fulfilled.

From now on, we focus on the local bifurcation analysis of S^+ due to the symmetry with respect to Π of these nontrivial singularities. Moreover, on the hypersurface $\mathcal{SN}$, the number of parameters are reduced from four to three: A, B, and λ_1.

The characteristic polynomial of the Jacobian matrix at S^+ associated to (5) can be written as $P(\mu) = \mu(\mu^3 + e_2\mu^2 + e_1\mu + e_0)$, where

$$\begin{aligned}
&e_2 = \tfrac{1}{\kappa_B^2}\left(4A^2(B^2+\kappa^2) - \kappa_B^2(B+1+4\lambda_1)\right),\\
&e_1 = \tfrac{1}{\kappa_B^3}\left(32A^4B\kappa^2 + \kappa_B^4(1+3\lambda_1)\right.\\
&\qquad \left.-8A^2\left(\kappa^3(2+5\lambda_1) + B^3\lambda_1 + B^2(2+9\lambda_1+10\lambda_1^2) + B\kappa^2(4+9\lambda_1)\right)\right),\\
&e_0 = \tfrac{4A^2\kappa^2}{\kappa_B^3}\left(\kappa^2(1+6\lambda_1) - B^3 + B^2(2\lambda_1-1) + B(1+8A^2+12\lambda_1+20\lambda_1^2)\right),
\end{aligned}$$

with $\kappa = \kappa(\lambda_1) = 1+2\lambda_1$ and $\kappa_B^i = (\kappa+B)^i$ for $i = 2, 3, 4$.

The surface

$$\mathcal{HZ} = \{(A, B, \lambda_1, \lambda_2) \in \mathcal{SN} :\ e_0 = e_1e_2,\ e_1 \geq 0\}$$

contains the Hopf-Zero bifurcations of codimension at least 2, i.e., parameter values where the Jacobian matrix at the equilibrium S^+ has a pair of pure imaginary eigenvalues and a zero eigenvalue.

Additionally, there exists another bifurcation surface on $\mathcal{SN}$ of codimension at least 2, $\mathcal{DZ} = \{(A, B, \lambda_1, \lambda_2) \in \mathcal{SN} :\ e_0 = 0\}$, on which the

Jacobian matrix of (5) at S^+ has a double zero eigenvalue with geometric multiplicity one and two additional eigenvalues $\mu_1 = \left(p + \sqrt{q}\right)/(4B)$ and $\mu_2 = \left(p - \sqrt{q}\right)/(4B)$, where

$$\begin{aligned} p &= 1 - B^3 + 10\lambda_1 + 28\lambda_1^2 + 24\lambda_1^3 + 3B^2(1+2\lambda_1) + B(1 + 4\lambda_1 - 4\lambda_1^2), \\ q &= B^6 - 6B^5(1+2\lambda_1) + (1+2\lambda_1)^4(1+6\lambda_1)^2 + B^4(-1 + 12\lambda_1 + 12\lambda_1^2) \\ &\quad + 4B^3(7 + 48\lambda_1 + 88\lambda_1^2 + 56\lambda_1^3) - B^2(1 + 48\lambda_1 + 184\lambda_1^2 + 256\lambda_1^3 + 80\lambda_1^4) \\ &\quad - 2B(1+2\lambda_1)^2(19 + 182\lambda_1 + 460\lambda_1^2 + 312\lambda_1^3). \end{aligned}$$

We can rewrite $\mathcal{DZ}$ as

$$\mathcal{DZ} = \left\{(A, B, \lambda_1, \lambda_2) \in \mathcal{SN} : \, A = \sqrt{B - 1 - 6\lambda_1}(B + 1 + 2\lambda_1)/(2\sqrt{2B})\right\}.$$

We have, except other degenerations hold, Bogdanov-Takens bifurcations.

On the other hand, the curve

$$\begin{aligned} \mathcal{HDZ} &= \{(A, B, \lambda_1, \lambda_2) \in \mathcal{SN} : e_0 = e_2 = 0, e_1 \geq 0\} \\ &= \{(A, B, \lambda_1, \lambda_2) \in \mathcal{DZ} : \; e_1 \geq 0, \\ &\quad B^3 - 3B^2(1+2\lambda_1) - (1+2\lambda_1)^2(1+6\lambda_1) + B(-1 - 4\lambda_1 + 4\lambda_1^2) = 0\}. \end{aligned}$$

contains the Hopf-Double-Zero bifurcation curve of codimension at least 3 (when the condition $e_1 > 0$ is fulfilled), i.e., parameter values where the Jacobian matrix at the equilibrium S^+ has a pair of pure imaginary eigenvalues and two zero eigenvalues. This type of singularities has been studied in [31, 36, 37].

On $\mathcal{DZ}$ there exists another bifurcation curve of codimension at least 3,

$$\begin{aligned} \mathcal{TZ} &= \{(A, B, \lambda_1, \lambda_2) \in \mathcal{SN} : \; e_0 = e_1 = 0\} \\ &= \{(A, B, \lambda_1, \lambda_2) \in \mathcal{DZ} : (1+2\lambda_1)^2(5 + 48\lambda_1 + 120\lambda_1^2 + 72\lambda_1^3) \\ &\quad + B(1 + 16\lambda_1 + 60\lambda_1^2 + 88\lambda_1^3 + 48\lambda_1^4) - B^2(3 + 22\lambda_1 + 48\lambda_1^2 + 40\lambda_1^3) \\ &\quad + B^3(1 + 2\lambda_1 + 4\lambda_1^2) = 0\}, \end{aligned}$$

on which the Jacobian matrix has at least three zero eigenvalues. The bifurcation diagram for these singularities was studied in [24, 25, 26].

Finally, on $\mathcal{TZ}$ there exists a unique Quadruple-Zero bifurcation point of codimension at least 4,

$$\begin{aligned}\mathcal{QZ} &= \{(A,B,\lambda_1,\lambda_2)\in\mathcal{SN} : e_0=e_1=e_2=0\}\\ &= \{(A,B,\lambda_1,\lambda_2)\in\mathcal{TZ} : B^3-3B^2(1+2\lambda_1)+B(-1-4\lambda_1+4\lambda_1^2)\\ &\quad-(1+2\lambda_1)^2(1+6\lambda_1)=0\}\,.\end{aligned}$$

An approximated value of the $\mathcal{QZ}$ bifurcation point is given by

$$\begin{aligned}A &\approx 2.6021429374, \quad B\approx 11.2982916304,\\ \lambda_1 &\approx 1.2506765846, \quad \lambda_2\approx 1.5159732650.\end{aligned}$$

In order to guarantee the existence and uniqueness of such a bifurcation point in a given interval, we use a simple Computer Assisted Proof (CAP) based on the Interval Newton method.

Theorem 2. *The CBS in (5) has a unique $\mathcal{QZ}$ bifurcation point in the interval $B = 11.2982916^{3169444}_{2903248}$ and $\lambda_1 = 1.250676584^{79589}_{35996}$.*

Proof. The $\mathcal{QZ}$ bifurcation point is a solution to $e_0=e_1=e_2=0$ in $\mathcal{SN}$. Moreover, from $e_0=e_1=0$, it follows that $\mathcal{QZ}\subset\mathcal{TZ}$. Then, the $\mathcal{QZ}$ bifurcation point satisfies

$$f(B,\lambda_1)=0, \tag{9}$$

where $f(B,\lambda_1) = ((1+2\lambda_1)^2(5+48\lambda_1+120\lambda_1^2+72\lambda_1^3)+B(1+16\lambda_1+60\lambda_1^2+88\lambda_1^3+48\lambda_1^4)-B^2(3+22\lambda_1+48\lambda_1^2+40\lambda_1^3)+B^3(1+2\lambda_1+4\lambda_1^2),\ B^3-3B^2(1+2\lambda_1)+B(-1-4\lambda_1+4\lambda_1^2)-(1+2\lambda_1)^2(1+6\lambda_1))$.

Using the interval Newton method [32] to the nonlinear system (9) and taking as first interval

$$Z = X \times Y = \{B \in [11.2982817, 11.2983017],\ \lambda_1 \in [1.2506666, 1.2506866]\}$$

we obtain

$$\begin{aligned} N(Z) &= Z_{mid} - [Df(Z)]^{-1} f(Z_{mid}) \\ &= \{[11.29829162903248, 11.29829163169444] \\ &\quad \times [1.25067658435996, 1.25067658479589]\} \subset Z, \end{aligned}$$

with Z_{mid} the midpoint of interval Z.

Hence, there exists a unique $(B^*, \lambda_1^*) \in N(Z)$ such that $f(B^*, \lambda_1^*) = 0$. All calculations were performed in MATLAB using the interval arithmetic toolbox INTLAB [33] and the code is provided in Appendix A. □

In [5], it was proved that the `CBS` generically unfolds a 4-dimensional singularity of codimension 4 at $\mathcal{QZ}$, which is an organizing center of chaotic dynamics. Particularly, there are values $(A, B, \lambda_1, \lambda_2)$ arbitrarily close to $\mathcal{QZ}$ for which, restricted to a normally attracting 3-dimensional invariant manifold, the `CBS` has Shilnikov homoclinic orbits and hence strange attractors.

In Figure 3, we sketch the set of bifurcations described above for the nontrivial singularity S^+.

3.3. Numerical exploration of the parameter space

To conclude this study of singularities and local bifurcations in the model, we explore numerically the parameter space. As our goal is to study if the chaotic regions `SM` and `DIR` are connected or not, we define a linking parameter $\alpha \in [0, 1]$ and a convex combination given by

$$A(\alpha) = \alpha A_1 + (1-\alpha) A_0, \quad \lambda_2(\alpha) = \alpha \lambda_{2,1} + (1-\alpha)\lambda_{2,0},$$

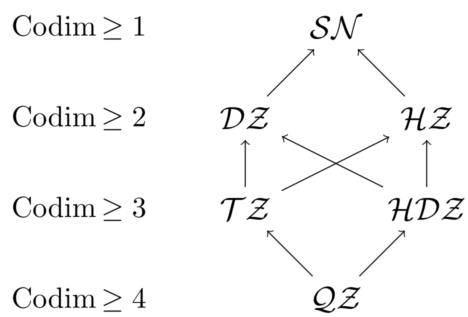

Figure 3: Saddle-Node ($\mathcal{SN}$), Double-Zero ($\mathcal{DZ}$), Hopf-Zero ($\mathcal{HZ}$), Triple-Zero ($\mathcal{TZ}$), Hopf-Double-Zero ($\mathcal{HDZ}$), and Quadruple-Zero ($\mathcal{QZ}$) bifurcations for the nontrivial singularity S^+.

α	$A = A(\alpha)$	$\lambda_2 = \lambda_2(\alpha)$
0	2	80
0.5	2.414406160565363	40.839862684029285
0.75	2.621609240848044	21.259794026043927
1	2.828812321130726	1.679725368058570

Table 1: Relevant parameter values for numerical exploration.

with $A_1 = 2.828812321130726, A_0 = 2, \lambda_{2,1} = 1.679725368058570$ and $\lambda_{2,0} = 80$, such that parameters corresponding to the chaotic region `SM` are obtained when $\alpha = 0$ and parameters corresponding to `DIR` when $\alpha = 1$. The parameter values used in this paper are summarized in Table 1.

Figure 4 shows, for different values of the linking parameter α, the color-coded parametric plane (B, λ_1) as a function of the number and type of equilibria. In particular, we record the number of equilibrium points and their corresponding stability in plots (D), (E), (F) and (A) for $\alpha = 0$, $\alpha = 0.5$, $\alpha = 0.75$ and $\alpha = 1$, respectively. In plots (B) and (C), two enlarged

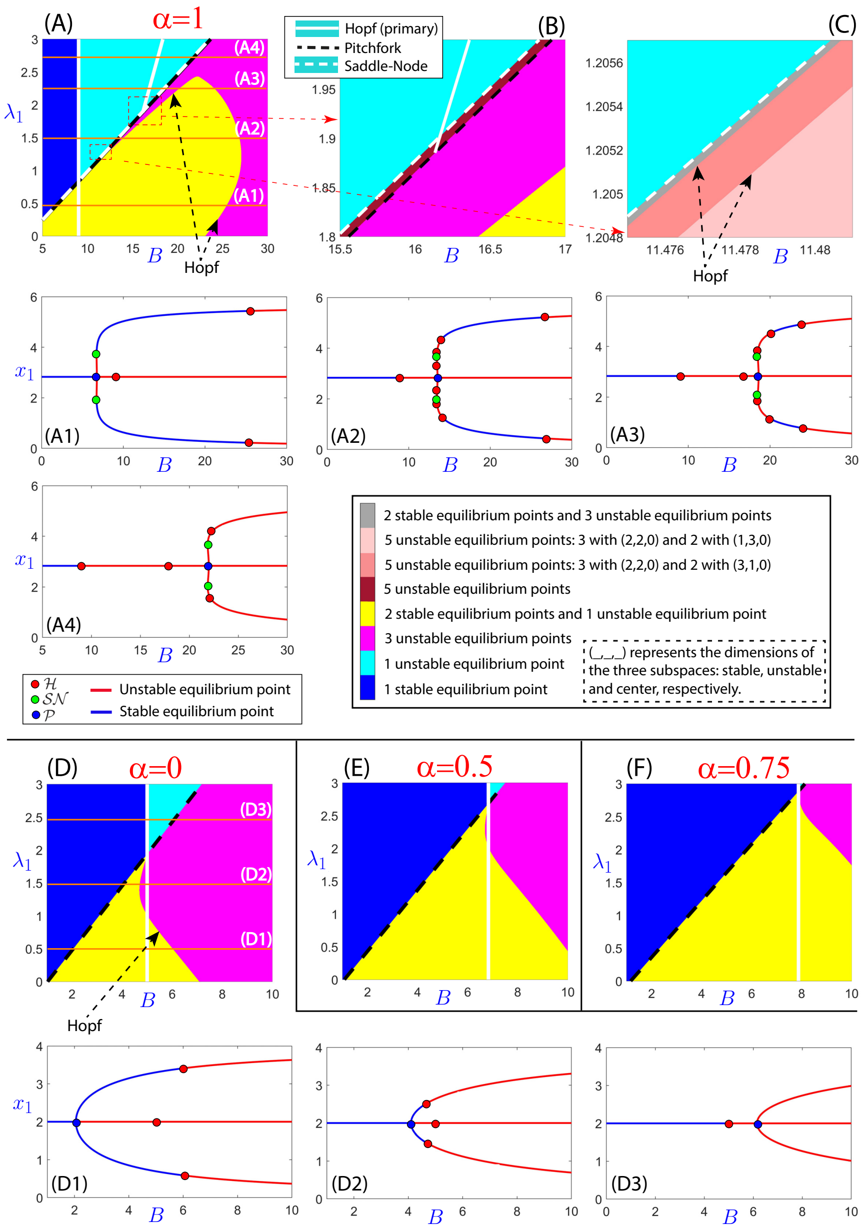

Figure 4: Color-coded regions with different number and type of equilibria, (A)-(F). Continuation analysis (performed with MatCont) for fixed λ_1, (A1)-(A4) and (D1)-(D3). See more details in the text.

areas of plot (A) are shown. The limit of each color region is associated with a particular bifurcation. For instance, a vertical white line corresponds to the Hopf bifurcation $\mathcal{H}_2$ while an oblique white line is related to the Hopf bifurcation $\mathcal{H}_1$. Moreover, a dashed black line represents the Pitchfork bifurcation $\mathcal{P}$ and a dashed white line is the Saddle-Node bifurcation $\mathcal{SN}$. The transition line between the yellow and magenta regions is associated with Hopf bifurcations of singularities $Q_\pm$. In (C), the transition lines between grey, dark pink and light pink regions are related with Hopf bifurcations of singularities $Q_\pm$ and $P_\pm$. In addition, we perform several one-parameter continuation studies for $\alpha = 0$ (see plots (D1)-(D3) for different values of λ_1 as indicated by horizontal orange lines in (D)) and $\alpha = 1$ (see plots (A1)-(A4) for different values of λ_1 as indicated by horizontal orange lines in (A)) in which the named bifurcations are represented with colored points.

In (D1) and (D2), which correspond to $\alpha = 0$, we observe three Hopf bifurcation points, two of them symmetric with respect to Π and located on the boundary between the yellow and magenta regions, and the other one on the vertical white line (associated to $\mathcal{H}_2$). The (B, λ_1) planes for $\alpha = 0.5$ and $\alpha = 0.75$ are very similar. In all these cases, we have a Pitchfork bifurcation $\mathcal{P}$. On the contrary, the system begins to have many more bifurcations when α is close to 1, mainly due to the proximity of high codimension bifurcations such as the Quadruple-Zero codimension-four bifurcation point $\mathcal{QZ}$. When $\alpha = 1$, there are more Hopf bifurcations (as we can see in (A2) and (A3)) that originate from the equilibria outside the invariant plane Π ($\mathcal{H}_3$ and $\mathcal{H}_4$ in Figure 5). Via cascades of period-doubling bifurcations, they may create several small chaotic regions.

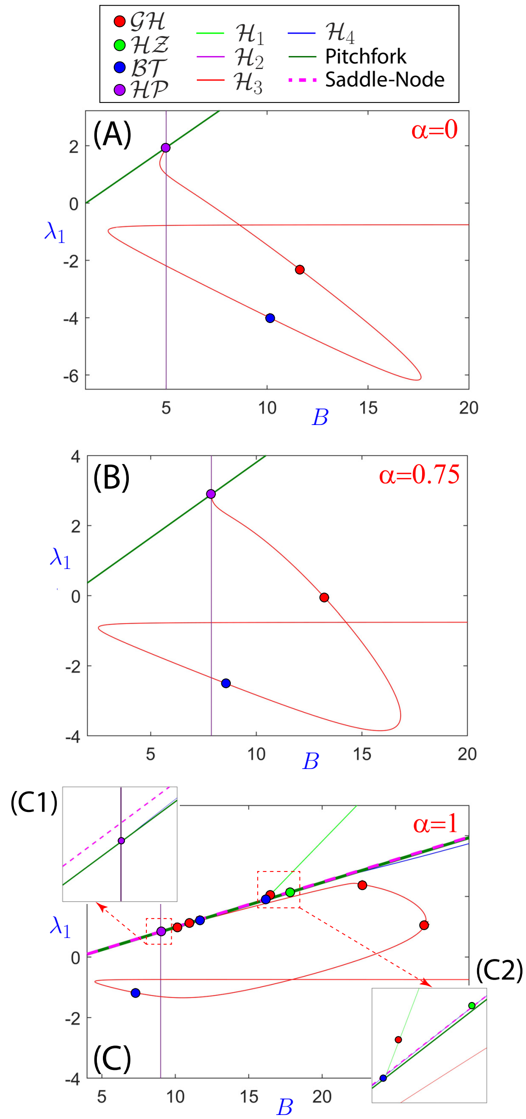

Figure 5: Biparametric continuations (performed with MatCont) in the (B, λ_1) plane for (A) $\alpha = 0$, (B) $\alpha = 0.75$ and (C) $\alpha = 1$. (C1)-(C2) are two enlarged regions of (C). See more details in the text.

Finally, in Figure 5 we present bifurcation diagrams in the plane (B, λ_1) for $\alpha = 0$, $\alpha = 0.75$ and $\alpha = 1$ to complete the study given in Figure 4.

Although all parameters in the model are positive, continuation extends through $\lambda_1 \leq 0$ to show a complete bifurcation diagram. Pitchfork ($\mathcal{P}$), Saddle-Node ($\mathcal{SN}$) and several Hopf bifurcation curves ($\mathcal{H}_1$, $\mathcal{H}_2$, $\mathcal{H}_3$ and $\mathcal{H}_4$) are shown in (A), (B) and (C). Generalized Hopf ($\mathcal{GH}$), Hopf-Zero ($\mathcal{HZ}$), Bogdanov-Takens ($\mathcal{BT}$) and Hopf-Pitchfork ($\mathcal{HP}$) bifurcation points in the graphs are also highlighted. In (C1) and (C2), we zoom in on two regions of plot (C) to correctly visualize the bifurcation points and curves.

4. Chaotic behavior: connections between organizing centers

In this section we provide numerical results that allow us to explore in detail the chaotic regions `SM` (the macro-chaos) and `DIR` (the micro-chaos) and study a possible connection between them. We utilize two main techniques to illustrate the different chaotic regions: the well-known Lyapunov exponents and the spike-counting method which consists in detecting the number of spikes (maxima) of the attracting limit cycles of the system.

Figures 6 and 7 show biparametric sweeps for different parametric planes. In the case of spike-counting maps, the darkest shade of blue indicates stationary behavior, the dark red regions are chaotic and each of the remaining colors is associated to periodic behavior with different number of spikes. In the Lyapunov exponents maps, the yellow-red color scale is used for the first positive Lyapunov exponent (chaotic region), while the gray scale is associated with first negative Lyapunov exponent and with the second Lyapunov exponent when the first is zero (regular behavior).

In Figure 6, (A) and (B) show biparametric sweeps in the plane (λ_1, λ_2), that contains the chaotic region `SM`, with the results of spike-counting technique and Lyapunov exponents. In this case, $A = 2$ and $B = 5.9$, which are the values given in [7]. As the analyses of this paper are performed in the biparametric plane (B, λ_1), we show the sweeps in such plane for the region `SM`. (C) and its enlarged regions (C1) and (C2) represent biparametric sweeps in the (B, λ_1) plane where the chaotic region `SM` is (the values A and λ_2 are fixed, see Table 1 for $\alpha = 0$). The magenta lines in (C1) are period-doubling ($\mathcal{PD}$) bifurcation curves that we obtain using the continuation software AUTO. We use the initial condition $(x_1, y_1, x_2, y_2) = (2.1, 2.9, 1.9, 3.0)$ to obtain all the panels. It is noteworthy that the chaotic region is of significant size and can be easily detected with standard techniques. In addition, typical "shrimp" structures can be observed within the chaotic region [34, 35].

If we study other parametric planes, chaotic regions are not present at all or they are very small. Most significantly, we may detect tiny chaotic regions by combining continuation techniques and theoretical studies, i.e., locating the appropriate high codimension bifurcation points to know where we should search. In Figure 7, we show how the parametric plane (B, λ_1) has, at least, two chaotic regions when A and λ_2 are fixed for $\alpha = 1$ (see Table 1). However, the size of these regions is so small (minimum and maximum values of the parameters vary in a range of the third-fourth decimal digit) that, without additional theoretical information, it would be impossible to detect them numerically.

In panels (A) and (B) of Figure 7, we apply the spike counting and the Lyapunov exponents techniques, respectively, in a neighborhood of the chaotic region `DIR`. A magnification of a part of the sweeping shown in (A) is given in (A1). Moreover, we present in (C) the spike-counting results in

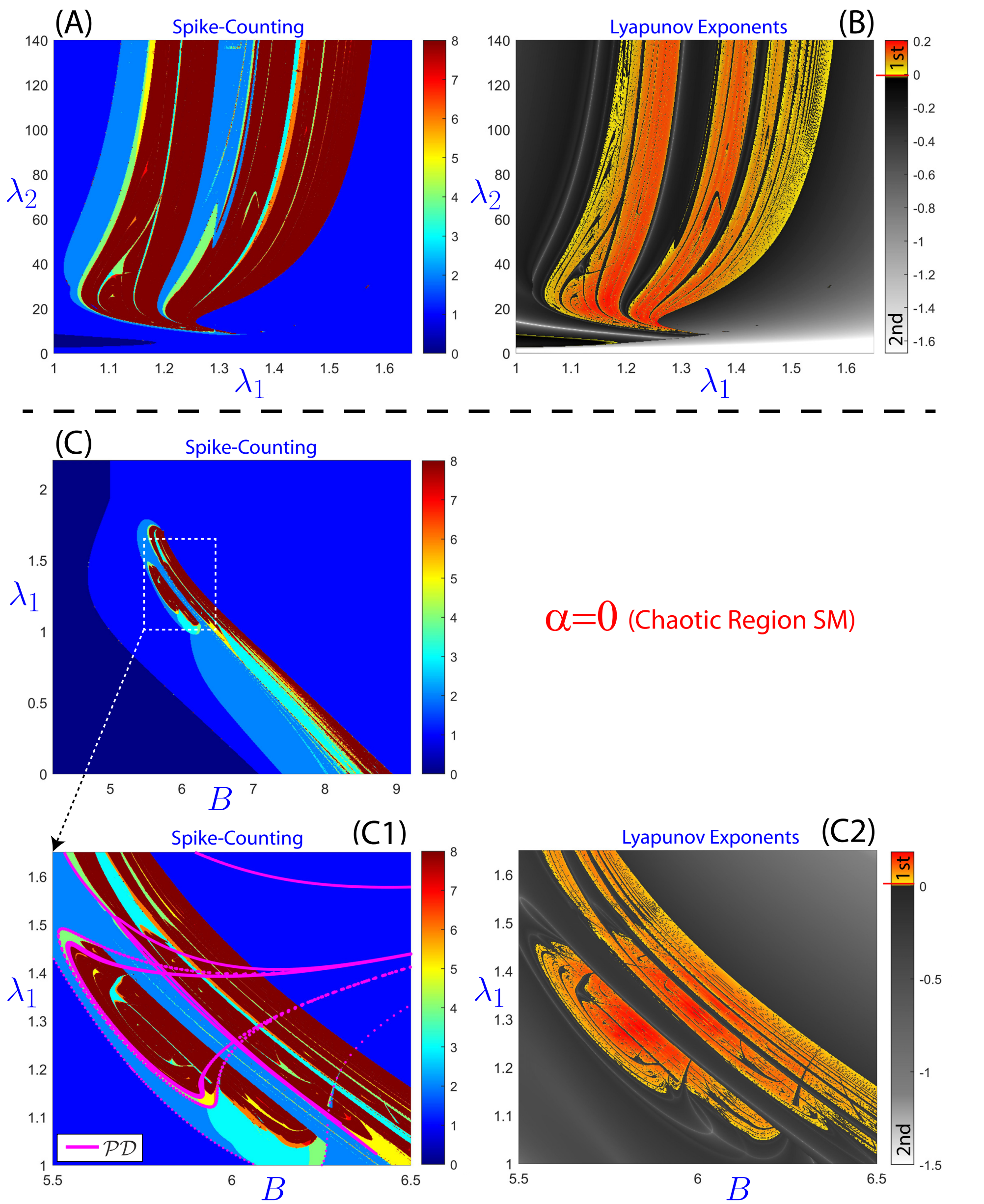

Figure 6: Spike-counting and Lyapunov exponents associated with the chaotic region SM in the parametric planes (λ_1, λ_2) and (B, λ_1). See more details in the text.

the (λ_1, λ_2) plane for $B = 11.4802$ and A fixed at the value $\alpha = 1$ (see Table 1). Here, the initial condition is set to $(x_1, y_1, x_2, y_2) = (2.057175842256981, 4.956812708388363, 3.600131217519688, 3.390639134503412)$. In any case, we emphasize that the detection of the chaotic region `DIR` relies heavily on the analytical results provided in [5]. Namely, in that paper it is proved that any generic unfolding of a $\mathcal{QZ}$ singularity includes generic unfoldings of Triple-Zero singularities where it has been proved that strange attractors are present. Moreover, in [5] it is proved that the `CBS` is a generic unfolding of the $\mathcal{QZ}$ point.

In Figure 7, (D) and (D1) correspond to a small chaotic region which is a continuation of region `SM`, the large chaotic zone contained in the (B, λ_1) plane with A and λ_2 fixed at the values provided in Table 1 for $\alpha = 0$. The initial condition is set to $(x_1, y_1, x_2, y_2) = (4.9683, 5.7519, 0.3418, 10.4385)$. In Figure 8, we show the numerical results that allow us to discover the tiny chaotic region connected to `SM`. They include different families of period-doubling curves shown in the parametric space (B, λ_1, α). First, we compute several period-doubling curves (blue, green and red) in the plane $\alpha = 0$ (those already shown in panel (C1) of Figure 6). We show how the red and green ones can be continued up to the horizontal plane $\alpha = 1$. To make this connection, some intermediate steps are required. In the case of the red curve, a total of five continuations are made. Three of them are continuations in horizontal planes $(\alpha = 0, 0.985, 1)$. For the other two, in order to move up in the vertical direction, convenient values of λ_1 are fixed. These consecutive continuations are necessary to deal with numerical difficulties, since a single continuation in (B, α) did not reach the plane $\alpha = 1$. The case of the green

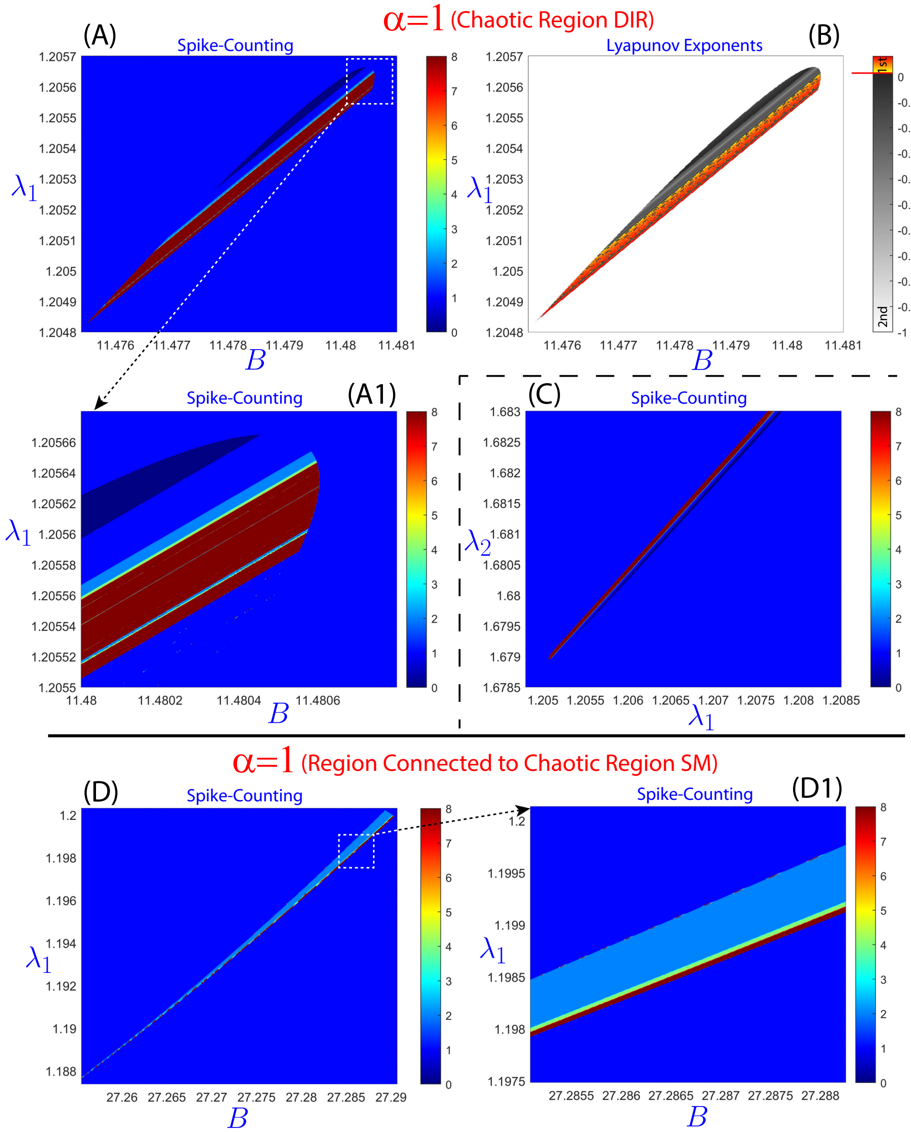

Figure 7: (A)-(C) Spike-counting and Lyapunov exponents associated with the chaotic region DIR in the parametric planes (B, λ_1) and (λ_1, λ_2). (D)-(D1) Spike-counting for a small chaotic region connected to SM in the parametric plane (B, λ_1). See more details in the text.

curve is similar but with more intermediate steps. The location of these period-doubling curves in the plane $\alpha = 1$ gives the region of the plane (B, λ_1) on which the numerical sweepings of panel (D) of Figure 7 were performed. In fact we see how a period-doubling curve (green) reaches the small chaotic region detected in the plane $\alpha = 1$, the one that connects with `SM`. Two additional period-doubling curves (purple) were computed in the plane $\alpha = 1$. All curves are included in panel (A) of Figure 8. The other panels contain projections in the planes (B, λ_1), (B, α) and (λ_1, α) for a better visualization. From this analysis we can conclude that chaotic regions `SM` and `DIR` are not connected (see panel (B) of Figure 8).

Finally, we notice that the location of attractors in the phase-space also provides information about their relevance in the dynamics of the coupled system. In panels (A)-(C) of Figure 9, we show the attracting invariant sets for the case $\alpha = 0$ (see Table 1) projected on the three-dimensional space (x_1, y_1, x_2), for a selection of values on the (B, λ_1)-plane. Firstly, two symmetric equilibrium points (in red) and a large limit cycle (in blue) on the invariant plane Π are observed in (A), where $B = 5.5$ and $\lambda_1 = 0.4$ (with initial condition $(x_1, y_1, x_2, y_2) = (1.425984, 3.180712, 1.425984, 3.180712)$ for the periodic orbit in the invariant plane Π, and $(x_1, y_1, x_2, y_2) = (3.421747, 1.825940, 0.578253, 1.857930)$ and its symmetric one respect to the invariant plane Π for the equilibrium points). Secondly, two symmetric periodic orbits (in red) and a large limit cycle (in blue) on Π are presented in (B), for $B = 5.602058319039463$ and $\lambda_1 = 1.2$ (with initial condition $(x_1, y_1, x_2, y_2) = (2.134227, 2.342226, 2.134227, 2.342226)$ for the orbit in Π, and $(x_1, y_1, x_2, y_2) = (1.978711, 1.046154, 6.691137, 0.966066)$ and its symmetric one for the pe-

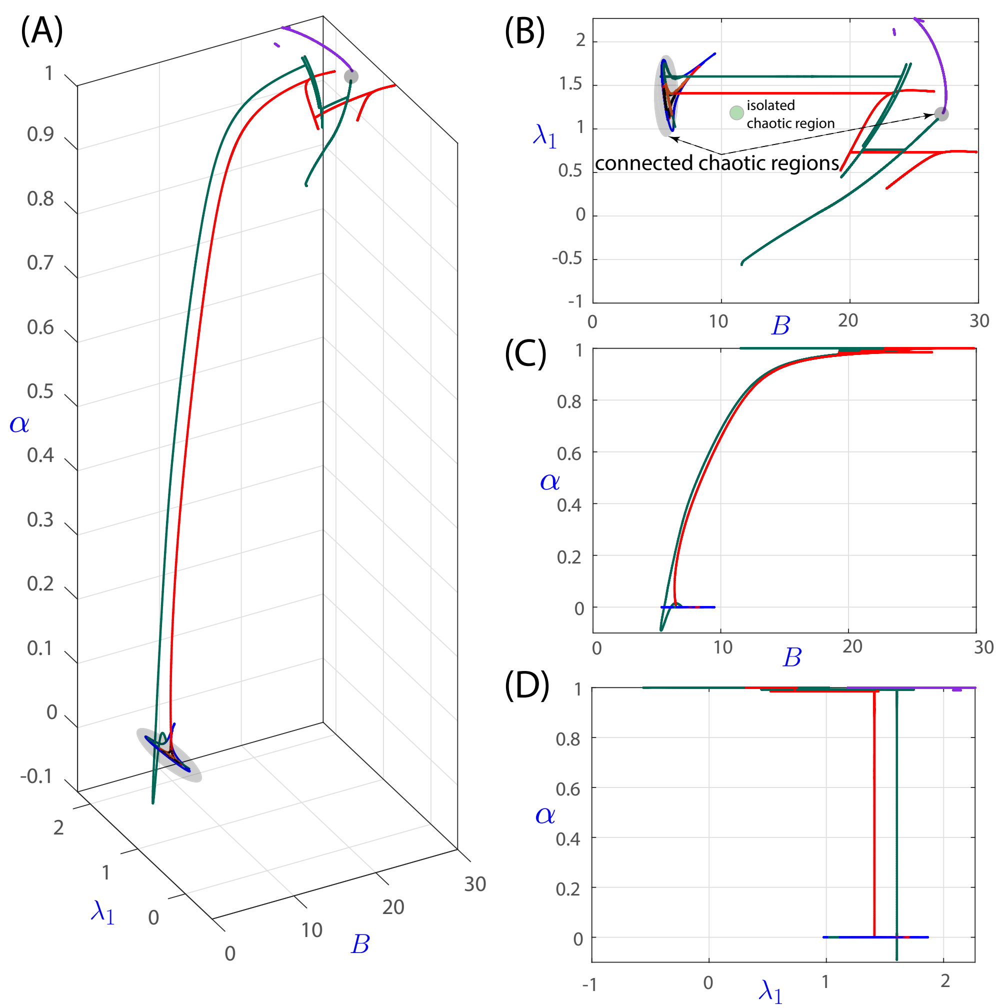

Figure 8: (A) Connection of period doubling bifurcation curves (performed with AUTO) from the plane $\alpha = 0$ (the one containing the region SM) to the plane $\alpha = 1$ (the one containing the region DIR) in the three-parameter space (B, λ_1, α). (B) Projection on the plane (B, λ_1) showing the position of the chaotic regions SM and DIR and also the region in the plane $\alpha = 1$ that connects with SM. Plots (C) and (D) show the (B, α) and (λ_1, α) planes, respectively, illustrating the connecting period-doubling bifurcations obtained using continuation techniques.

riodic orbits outside the invariant plane). And thirdly, two symmetric chaotic attractors (in red and green) and a large limit cycle on the plane Π (in blue) are shown in (C), where $B = 6.375300171526684$ and $\lambda_1 = 1.2$ (with initial condition $(x_1, y_1, x_2, y_2) = (3.730940, 1.626618, 3.730940, 1.626618)$ for the periodic orbit in Π, and $(x_1, y_1, x_2, y_2) = (2.1, 2.9, 1.9, 3.0)$ and its symmetric one for the chaotic attractors). In plots (A1), (B1) and (C1), the (x_1, x_2) projection of the attractors is shown to observe the symmetry more clearly. We highlight that, in this case, the periodic orbits and the chaotic attractors are all of similar size and share common regions in the phase-space. In panels (D)-(F) of Figure 9, we show the attracting invariant sets for the case $\alpha = 1$ (see Table 1). First, two symmetric equilibrium points (in red) and a periodic orbit (in blue) on the invariant plane Π are presented in (D), for $B = 11.479226348021538$ and $\lambda_1 = 1.2055$ (with initial condition $(x_1, y_1, x_2, y_2) = (0.309490, 11.193851, 0.309490, 11.193851)$ for the periodic orbit in the invariant plane Π, and $(x_1, y_1, x_2, y_2) = (1.990186, 5.045707, 3.667439, 3.342718)$ and its symmetric one respect to the invariant plane Π for the equilibrium points). Second, two symmetric periodic orbits (in red) and a periodic orbit (in blue) on the invariant plane Π are shown in (E), for $B = 11.479461517086209$ and $\lambda_1 = 1.2055$ (with initial condition $(x_1, y_1, x_2, y_2) = (0.309490, 11.193851, 0.309490, 11.193851)$ for the orbit in Π, and $(x_1, y_1, x_2, y_2) = (1.970296, 5.072571, 3.691614, 3.324793)$ and its symmetric one for the periodic orbits outside the invariant plane Π). In (D1) and (E1), the projection on the plane (x_1, x_2) of such attractors is given. (E2) is an enlargement of a region of (E1) to show that the red marks are, in fact, periodic orbits. Next, we represent together in (F) the attractors for two different values of

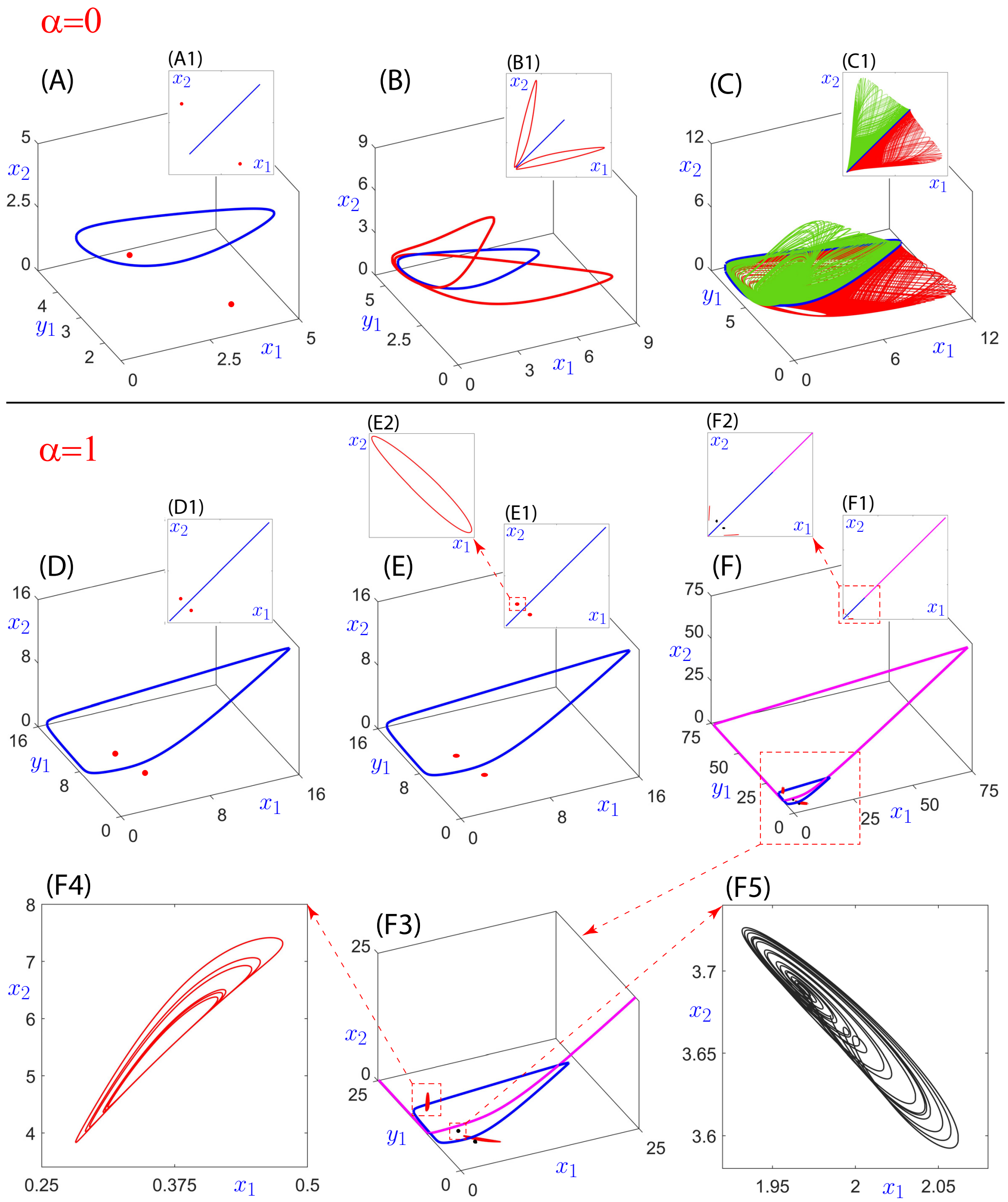

Figure 9: Different orbits in the two regions $\alpha = 0$ (SM) and $\alpha = 1$ (DIR and region connected to SM). See more details in the text.

the parameters B and λ_1. Thus, we can compare the chaotic attractors detected in `DIR` (setting $B = 11.479799259891854$, $\lambda_1 = 1.2055$, and the initial conditions $(x_1, y_1, x_2, y_2) = (2.057176, 4.956813, 3.600131, 3.390639)$ and its symmetric one respect to Π) with those that we found in the chaotic region connected to `SM` (setting $B = 27.287198018812745$, $\lambda_1 = 1.198739299073543$, and the initial conditions $(x_1, y_1, x_2, y_2) = (4.9683, 5.7519, 0.3418, 10.4385)$ and its symmetric one respect to the invariant plane). Namely, there are two periodic orbits on the invariant plane Π (in blue and magenta) and two pairs of symmetric chaotic attractors with respect to Π (in black, the attractor of `DIR`; and in red, the one of the chaotic region connected to `SM`). We set the initial condition $(x_1, y_1, x_2, y_2) = (0.309490, 11.193851, 0.309490, 11.193851)$ for the blue periodic orbit, whose parameter values coincide with those used for the chaotic attractor of `DIR`. For the magenta periodic orbit, the parameter values are the ones used to represent the chaotic attractor of the chaotic region connected to `SM`, and the initial conditions are $(x_1, y_1, x_2, y_2) = (0.106083, 15.390842, 0.106083, 15.390842)$ and its symmetric. In (F1) and in the enlargement (F2), the projection on the plane (x_1, x_2) of attractors is shown. In (F3), we zoom in on the pointed zone in (F) to have a better image of the attractors. In (F4) and (F5), (x_1, x_2) projections of the chaotic attractors for the different parameter values are given. The chaotic attractor in (F5) is related to the chaotic region `DIR` while the one in (F4) corresponds to this of the chaotic region connected to `SM`. Notably, one can observe how in the case of $\alpha = 1$ the periodic orbits and the chaotic attractors are of different magnitude. Essentially, the (periodic) attractors located on the plane of symmetry are much larger.

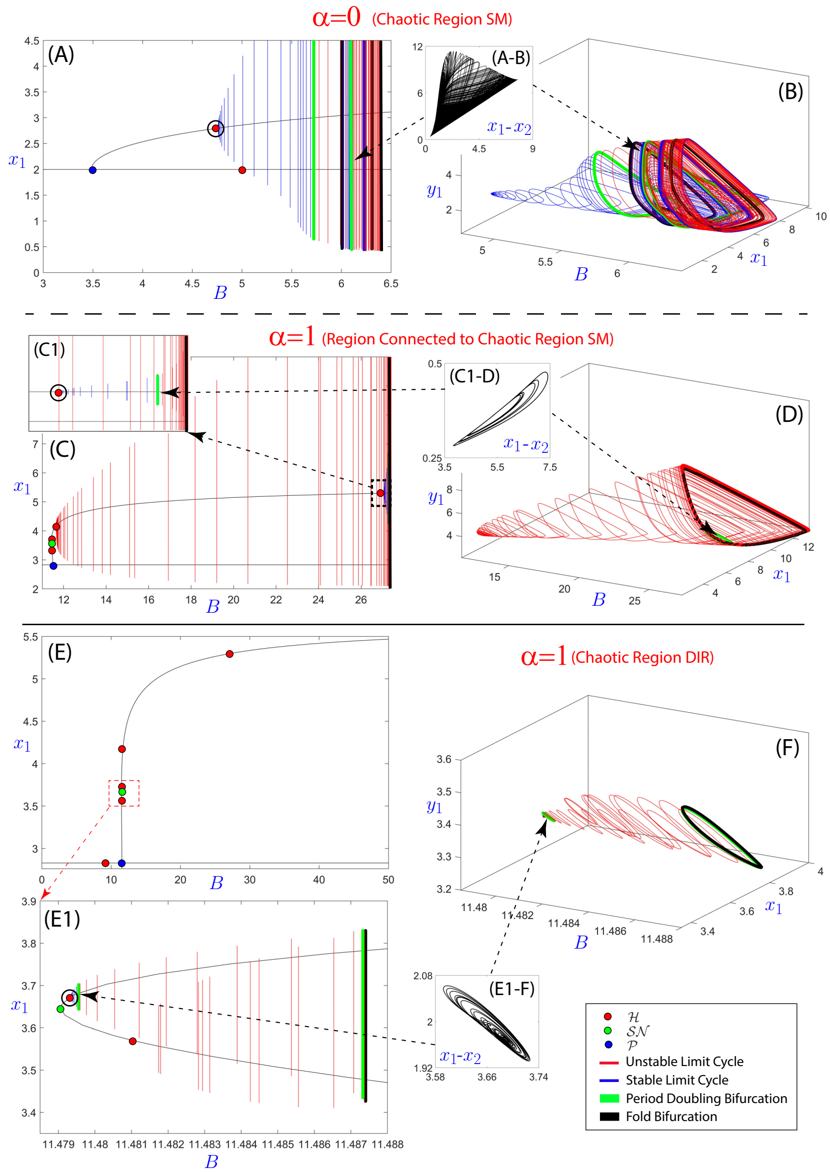

Figure 10: Routes to three different chaotic regions via Hopf (red points circled in black) and cascades of period-doubling bifurcations. $\lambda_1 = 1.2$, 1.198739299073543, 1.2055 for the continuations (performed with MATCONT) of chaotic region SM, the one connected to SM, and region DIR, respectively. See more details in the text.

The three different chaotic regions studied in this paper (`SM`, `DIR` and the region connected to `SM` when $\alpha = 1$) are generated through classical period-doubling bifurcations initiated on limit cycles arising in Hopf bifurcations. In Figure 10, we show the continuation of these periodic orbits and we locate the first period-doubling (in green) and fold bifurcations (in black) of limit cycles. In (A), we present the results of the one-parameter continuation on the (B, x_1) plane for $\alpha = 0$ (see Table 1). Indeed, we locate the Hopf bifurcation points and show the stable limit cycles created at the supercritical Hopf bifurcation that will give rise later to a cascade of period-doubling bifurcations that leads to the chaotic region `SM`. A 3D image of the limit cycles in the (x_1, B, y_1) space is presented in (B) and a chaotic attractor is shown in (A-B). We provide similar images in (C), (C1), (D) and (C1-D) but for the chaotic region connected to `SM` for $\alpha = 1$. We should notice that both the size of the chaotic region and the chaotic attractor itself are really small, contrary to the case $\alpha = 0$, where they are quite large and therefore easy to detect numerically. In (E), (E1), (F) and (E1-F), we present similar images but in the chaotic region `DIR` (with $\alpha = 1$, see Table 1). We zoom in on a region of (E) to correctly visualize in (E1) the limit cycles of the Hopf bifurcation that generates the chaotic region `DIR`. We can see that the parametric region is now much smaller than in the previous cases.

Conclusions

The `CBS` model is a nice example of how chaos can emerge when two simple dynamics (identical oscillations) are coupled by means of a simple mechanism of interaction (linear diffusion). Two chaotic regions are known from the literature, the first (SM) detected in [7] only with numerical techniques, and the second (DIR) found in [5] exploring numerically the neighborhood of a singularity for which theory predicts the genesis of strange attractors in any generic unfolding. To study a possible connection between both chaotic regions, we introduce a linking parameter $\alpha \in [0, 1]$ and a family of (B, λ_1) planes in the $(A, B, \lambda_1, \lambda_2)$-space such that the plane for $\alpha = 0$ contains the region SM and the one for $\alpha = 1$, the region DIR. Our numerical exploration of such a three-parameter family shows no connection between those chaotic regions. Of course, this is not surprising since a family of dynamical systems may exhibit disjoint chaotic regions. The interest of finding a connection between those chaotic regions was in fact to establish a link between the chaotic region SM and a singularity.

In our study we conclude that DIR is quite small and it could remain hidden for numerical exploration unless theoretical results were used. Therefore, the study of singularities is not only useful to prove the existence of chaos, as it can also help to locate small chaotic regions. Furthermore, as it follows from Section 3, the CBS exhibits a very rich map of singularities. Some of them, and not only Triple-Zero singularities, unfold chaotic behaviors. This is the case of Hopf-Zero singularities (see [28, 29]), Hopf-Pitchfork singularities (see explanations in [10]) and Hopf-Double-Zero singularities (see details in [36, 37]), all of them present in the CBS. It might be also interesting to analyze the size that the chaotic regions arising from these organizing centers can achieve. More importantly, although the size of DIR is small, other Triple-Zero singularities may unfold larger chaotic regions.

It is clear that the bifurcation diagrams of the CBS model (3) show a notorious complexity and deeper explorations could be of great interest. A more detailed study of local and global bifurcations on the invariant plane $\Pi = \{x_1 = x_2, y_1 = y_2\}$ is particularly relevant and will be a topic for future research. Note that orbits on Π correspond to synchronized solutions. Most significantly, all attractors contained in Π or close enough to Π are related with the synchronization phenomena exhibited in the model and, certainly, many of these attractors will be unfolded by singularities located on the invariant plane.

Acknowledgments

RB was supported by the Spanish Research projects PGC2018-096026-B-I00 and PID2021-122961NB-I00, and the European Regional Development Fund and Diputación General de Aragón (E24-17R and LMP124-18). FD, LP and SI were supported by the Grant PID2020-113052GB-I00 funded by MCIN/AEI/10.13039/501100011033. FD was supported by the Spanish Research project PID2021-122961NB-I00. LP was supported in part by the Gobierno de Asturias project PA-18-PF-BP17-072. AM was supported by the Spanish Research projects PGC2018-096026-B-I00 and PID2021-122961NB-I00 and Diputación General de Aragón E24-17R. CM was supported by Ministerio de Universidades of Spain with an FPU grant (FPU20/04039) and by the Spanish Research projects PGC2018-096026-B-I00 and PID2021-122961NB-I00. AL was supported by the Spanish Research project PGC2018-096026-B-I00 and PID2021-122961NB-I00 and Diputación General de Aragón (E22-20R). JJ was supported by the Spanish Research project PID2021-122961NB-I00.

Appendix A. INTLAB code for the CAP of the existence of the Quadruple-Zero bifurcation point

```
format compact long infsup
% System
f = @(B, lam1) [(1+2*lam1)^2*(5+48*lam1+120*lam1^2+72*lam1^3)+...
    B*(1+16*lam1+60*lam1^2+88*lam1^3+48*lam1^4)-...
    B^2*(3+22*lam1+48*lam1^2+40*lam1^3)+...
    B^3*(1+2*lam1+4*lam1^2),...
    B^3-3*B^2*(1+2*lam1)+B*(-1-4*lam1+4*lam1^2)-...
    (1+2*lam1)^2*(1+6*lam1)];
% Interval for B
X = midrad(11.2982917, 1e-5);
% Interval for lam1
Y = midrad(1.2506766, 1e-5);
% Interval Newton method
intervalNewtonMethod_Brusselator(f, X, Y)

function intervalNewtonMethod_Brusselator(f, X, Y)
% Mid point of the interval
mid_point= infsup([mid(X) mid(Y)], [mid(X) mid(Y)]);
% f(mid_point)
f_mid_point = intval(f(sup(mid_point(1,1)), sup(mid_point(1,2))));
% Jacobian matrix
Jac = @(B, lam1)[16*lam1-2*B*(40*lam1^3+48*lam1^2+22*lam1+3)+...
    3*B^2*(4*lam1^2+2*lam1+1)+60*lam1^2+88*lam1^3+48*lam1^4+1,...
    (8*lam1+4)*(72*lam1^3+120*lam1^2+48*lam1+5)+...
    B*(192*lam1^3+264*lam1^2+120*lam1+16)+B^3*(8*lam1+2)+...
    (2*lam1+1)^2*(216*lam1^2+240*lam1+48)-B^2*(120*lam1^2+96*lam1+22);...
    3*B^2-4*lam1+4*lam1^2-6*B*(2*lam1+1)-1,...
    B*(8*lam1-4)-6*B^2-(6*lam1+1)*(8*lam1+4)-6*(2*lam1+1)^2];
```

```
% Evaluation of the Jacobian matrix
Jac_XY = intval(Jac(X, Y));
% Inverse of the Jacobian matrix
inv_Jac_XY = intval(inv(Jac_XY));
% N
N = mid_point.' - inv_Jac_XY * f_mid_point.';
% Computation of the intersection
newX = intersect(N(1, 1), X);
newY = intersect(N(2, 1), Y);
if newX==N(1, 1) && newY==N(2, 1) && N(1, 1)~=X && N(2, 1)~=Y
    % There exists a unique solution in N
    disp('Unique solution in N')
    disp(N)
elseif isnan(newX) || isnan(newY)
    % There is no solution in the interval
    disp('No solution in the interval')
else
    % We keep looking for the solution
    intervalNewtonMethod_Brusselator(f, newX, newY)
end
end
```

References

[1] A. M. Turing, The chemical basis of morphogenesis, Phil. Trans. R. Soc. Lond. B 237 (641) (1952) 37–72. doi:10.1098/rstb.1952.0012.

[2] S. Smale, A mathematical model of two cells via Turing's equation, Springer New York, 1976, pp. 354–367. doi:10.1007/978-1-4612-6374-6_24.

[3] L. N. Howard, Nonlinear oscillations, in: Nonlinear Oscillations in Biology (Proc. Tenth Summer Sem. Appl. Math., Univ. Utah, Salt Lake City, Utah, 1978), Vol. 17 of Lectures in Appl. Math., Amer. Math. Soc., Providence, R.I., 1979, pp. 1–67.

[4] J. C. Alexander, Spontaneous oscillations in two 2-component cells coupled by diffusion, Journal of Mathematical Biology 23 (2) (1986) 205–219. doi:10.1007/BF00276957.

[5] F. Drubi, S. Ibáñez, J. A. Rodríguez, Coupling leads to chaos, J. Differential Equations 239 (2) (2007) 371–385. doi:10.1016/j.jde.2007.05.024.

[6] G. Nicolis, I. Prigogine, Self-organization in nonequilibrium systems. From dissipative structures to order through fluctuations, The Quarterly Review of Biology 53 (3) (1978) 362–363. doi:10.1086/410785.

[7] I. Schreiber, M. Marek, Strange attractors in coupled reaction-diffusion cells, Physica D: Nonlinear Phenomena 5 (2) (1982) 258–272. doi:10.1016/0167-2789(82)90021-5.

[8] A. Dhooge, W. Govaerts, Y. A. Kuznetsov, H. G. E. Meijer, B. Sautois, New features of the software MatCont for bifurcation analysis of dynamical systems, MCMDS 14 (2) (2008) 147–175.

[9] F. Drubi, S. Ibáñez, J. A. Rodríguez, Singularities and chaos in coupled systems, Bull. Belg. Math. Soc. Simon Stevin 15 (5, Dynamics in perturbations) (2008) 797–808. doi:10.36045/bbms/1228486408.

[10] F. Drubi, S. Ibáñez, J. A. Rodríguez, Hopf-Pitchfork singularities in

coupled systems, Physica D: Nonlinear Phenomena 240 (9) (2011) 825–840. doi:10.1016/j.physd.2010.12.013.

[11] E. J. Doedel, R. C. Paffenroth, A. R. Champneys, T. F. Fairgrieve, Y. A. Kuznetsov, B. E. Oldeman, B. Sandstede, X. J. Wang, Auto2000, http://cmvl.cs.concordia.ca/auto.

[12] R. Barrio, S. Serrano, A three-parametric study of the Lorenz model, Physica D: Nonlinear Phenomena 229 (1) (2007) 43–51.

[13] R. Barrio, F. Blesa, S. Serrano, Qualitative analysis of the Rössler equations: Bifurcations of limit cycles and chaotic attractors, Physica D: Nonlinear Phenomena 238 (13) (2009) 1087–1100.

[14] J. A. Gallas, Non-quantum chirality in a driven Brusselator, Journal of Physics: Condensed Matter 34 (14) (2022) 144002.

[15] F. Drubi, S. Ibáñez, P. Pilarczyk, Nilpotent singularities and chaos: Tritrophic food chains, Chaos, Solitons & Fractals 142 (2020) 110406. doi:10.1016/j.chaos.2020.110406.

[16] M. Benedicks, L. Carleson, The dynamics of the Hénon map, Ann. of Math. (2) 133 (1) (1991) 73–169. doi:10.2307/2944326.

[17] L. Mora, M. Viana, Abundance of strange attractors, Acta Math. 171 (1) (1993) 1–71. doi:10.1007/BF02392766.

[18] L. P. Shilnikov, A case of the existence of a denumerable set of periodic motions, Dokl. Akad. Nauk SSSR 160 (1965) 558–561.

[19] L. P. Shilnikov, A contribution to the problem of the structure of an extended neighborhood of a rough equilibrium state of saddle-focus type, Math. USSR, Sb. 10 (1970) 91–102. doi:10.1070/sm1970v010n01abeh001588.

[20] C. Tresser, About some theorems by LP Šil'nikov, Annales de l'I.H.P. Physique théorique 40 (4) (1984) 441–461.

[21] A. J. Homburg, Periodic attractors, strange attractors and hyperbolic dynamics near homoclinic orbits to saddle-focus equilibria, Nonlinearity 15 (4) (2002) 1029–1050. doi:10.1088/0951-7715/15/4/304.

[22] A. Pumariño, J. A. Rodríguez, Coexistence and persistence of strange attractors, Vol. 1658 of Lect. Notes Math., Springer-Verlag, Berlin, 1997. doi:10.1007/BFb0093337.

[23] A. Pumariño, J. A. Rodríguez, Coexistence and persistence of infinitely many strange attractors, Ergodic Theory Dynam. Systems 21 (5) (2001) 1511–1523. doi:10.1017/S0143385701001730.

[24] S. Ibáñez, J. A. Rodríguez, Shil'nikov configurations in any generic unfolding of the nilpotent singularity of codimension three on $\mathbb{R}^3$, J. Differential Equations 208 (1) (2005) 147–175. doi:10.1016/j.jde.2003.08.006.

[25] F. Dumortier, S. Ibáñez, H. Kokubu, New aspects in the unfolding of the nilpotent singularity of codimension three, Dyn. Syst. 16 (1) (2001) 63–95. doi:10.1080/02681110010017417.

[26] F. Dumortier, S. Ibáñez, H. Kokubu, Cocoon bifurcation in three-dimensional reversible vector fields, Nonlinearity 19 (2) (2006) 305–328. doi:10.1088/0951-7715/19/2/004.

[27] P. G. Barrientos, S. Ibáñez, J. A. Rodríguez, Heteroclinic cycles arising in generic unfoldings of nilpotent singularities, J. Dynam. Differential Equations 23 (4) (2011) 999–1028. doi:10.1007/s10884-011-9230-5.

[28] I. Baldomá, S. Ibáñez, T. M. Seara, Hopf-Zero singularities truly unfold chaos, Commun. Nonlinear Sci. Numer. Simul. 84 (2020) 105162. doi:10.1016/j.cnsns.2019.105162.

[29] F. Dumortier, S. Ibáñez, H. Kokubu, C. Simó, About the unfolding of a Hopf-Zero singularity, Discrete Contin. Dyn. Syst. 33 (10) (2013) 4435–4471. doi:10.3934/dcds.2013.33.4435.

[30] A. Arneodo, P. Coullet, E. Spiegel, C. Tresser, Asymptotic chaos, Physica D: Nonlinear Phenomena 14 (3) (1985) 327–347. doi:10.1016/0167-2789(85)90093-4.

[31] W. F. Langford, K. Zhan, Interactions of Andronov-Hopf and Bogdanov-Takens bifurcations, in: The Arnoldfest (Toronto, ON, 1997), Vol. 24 of Fields Inst. Commun., Amer. Math. Soc., Providence, RI, 1999, pp. 365–383.

[32] R. E. Moore, R. B. Kearfott, M. J. Cloud, Introduction to interval analysis, SIAM, 2009.

[33] S. M. Rump, INTLAB - INTerval LABoratory, in: T. Csendes (Ed.), Developments in Reliable Computing, Kluwer Academic Publishers, Dordrecht, 1999, pp. 77–104, `http://www.tuhh.de/ti3/rump/`.

[34] C. Bonatto, J. C. Garreau, J. A. C. Gallas, Self-similarities in the frequency-amplitude space of a loss-modulated CO_2 laser, Phys. Rev. Lett. 95 (2005) 143905. doi:10.1103/PhysRevLett.95.143905.

[35] C. Bonatto, J. A. C. Gallas, Periodicity hub and nested spirals in the phase diagram of a simple resistive circuit, Phys. Rev. Lett. 101 (2008) 054101. doi:10.1103/PhysRevLett.101.054101.

[36] F. Drubi, S. Ibáñez, D. Rivela, A formal classification of Hopf-Bogdanov-Takens singularities of codimension three, J. Math. Anal. Appl. 480 (2) (2019) 123408, 15. doi:10.1016/j.jmaa.2019.123408.

[37] F. Drubi, S. Ibáñez, D. Rivela, Chaotic behavior in the unfolding of Hopf-Bogdanov-Takens singularities, Discrete Contin. Dyn. Syst. Ser. B 25 (2) (2020) 599–615. doi:10.3934/dcdsb.2019256.